NASA/TM—2010-216738

Validation of Heat Transfer and Film Cooling Capabilities of the 3–D RANS Code TURBO

Vikram Shyam
Glenn Research Center, Cleveland, Ohio

Ali Ameri and Jen-Ping Chen
The Ohio State University, Columbus, Ohio

June 2010

NASA STI Program . . . in Profile

Since its founding, NASA has been dedicated to the advancement of aeronautics and space science. The NASA Scientific and Technical Information (STI) program plays a key part in helping NASA maintain this important role.

The NASA STI Program operates under the auspices of the Agency Chief Information Officer. It collects, organizes, provides for archiving, and disseminates NASA's STI. The NASA STI program provides access to the NASA Aeronautics and Space Database and its public interface, the NASA Technical Reports Server, thus providing one of the largest collections of aeronautical and space science STI in the world. Results are published in both non-NASA channels and by NASA in the NASA STI Report Series, which includes the following report types:

- TECHNICAL PUBLICATION. Reports of completed research or a major significant phase of research that present the results of NASA programs and include extensive data or theoretical analysis. Includes compilations of significant scientific and technical data and information deemed to be of continuing reference value. NASA counterpart of peer-reviewed formal professional papers but has less stringent limitations on manuscript length and extent of graphic presentations.

- TECHNICAL MEMORANDUM. Scientific and technical findings that are preliminary or of specialized interest, e.g., quick release reports, working papers, and bibliographies that contain minimal annotation. Does not contain extensive analysis.

- CONTRACTOR REPORT. Scientific and technical findings by NASA-sponsored contractors and grantees.

- CONFERENCE PUBLICATION. Collected papers from scientific and technical conferences, symposia, seminars, or other meetings sponsored or cosponsored by NASA.

- SPECIAL PUBLICATION. Scientific, technical, or historical information from NASA programs, projects, and missions, often concerned with subjects having substantial public interest.

- TECHNICAL TRANSLATION. English-language translations of foreign scientific and technical material pertinent to NASA's mission.

Specialized services also include creating custom thesauri, building customized databases, organizing and publishing research results.

For more information about the NASA STI program, see the following:

- Access the NASA STI program home page at *http://www.sti.nasa.gov*

- E-mail your question via the Internet to *help@sti.nasa.gov*

- Fax your question to the NASA STI Help Desk at 443–757–5803

- Telephone the NASA STI Help Desk at 443–757–5802

- Write to:
  NASA Center for AeroSpace Information (CASI)
  7115 Standard Drive
  Hanover, MD 21076–1320

NASA/TM—2010-216738

Validation of Heat Transfer and Film Cooling Capabilities of the 3–D RANS Code TURBO

Vikram Shyam
Glenn Research Center, Cleveland, Ohio

Ali Ameri and Jen-Ping Chen
The Ohio State University, Columbus, Ohio

National Aeronautics and
Space Administration

Glenn Research Center
Cleveland, Ohio 44135

June 2010

This work was sponsored by the Fundamental Aeronautics Program at the NASA Glenn Research Center.

Level of Review: This material has been technically reviewed by technical management.

Available from

NASA Center for Aerospace Information
7115 Standard Drive
Hanover, MD 21076–1320

National Technical Information Service
5301 Shawnee Road
Alexandria, VA 22312

Available electronically at http://gltrs.grc.nasa.gov

Validation of Heat Transfer and Film Cooling Capabilities of the 3–D RANS Code TURBO

Vikram Shyam
National Aeronautics and Space Administration
Glenn Research Center
Cleveland, Ohio 44135

Ali Ameri and Jen-Ping Chen
The Ohio State University
Columbus, Ohio 43210

Abstract

The capabilities of the 3–D unsteady RANS code TURBO have been extended to include heat transfer and film cooling applications. The results of simulations performed with the modified code are compared to experiment and to theory, where applicable. Wilcox's *k*-ω turbulence model has been implemented to close the RANS equations. Two simulations are conducted: (1) flow over a flat plate and (2) flow over an adiabatic flat plate cooled by one hole inclined at 35° to the free stream. For (1) agreement with theory is found to be excellent for heat transfer, represented by local Nusselt number, and quite good for momentum, as represented by the local skin friction coefficient. This report compares the local skin friction coefficients and Nusselt numbers on a flat plate obtained using Wilcox's *k*-ω model with the theory of Blasius. The study looks at laminar and turbulent flows over an adiabatic flat plate and over an isothermal flat plate for two different wall temperatures. It is shown that TURBO is able to accurately predict heat transfer on a flat plate. For (2) TURBO shows good qualitative agreement with film cooling experiments performed on a flat plate with one cooling hole. Quantitatively, film effectiveness is under predicted downstream of the hole.

Introduction

TURBO

TURBO is an unsteady, viscous, 3–D RANS code. A modified high order, upwind Roe scheme is employed for spatial discretization with Newton sub-iterations to converge the solution at every time step. Due to the upwinding scheme used in this simulation there is no addition of artificial dissipation. The code is fully parallelized to use Message Passing Interface (MPI) (Refs. 1 and 2). The code was designed to simulate axial flows and therefore had several limitations. In the following list, i, j, and k are the indices of the computational coordinates.

- The inlet face must be at i_{min}
- The exit face must be at i_{max}
- The inlet and exit should be in the axial (x) direction.
- Periodic surfaces should be constant k surfaces
- The j index represents the radial direction with j_{min} being the hub surface and j_{max} the casing. In a rotating simulation only the j_{max} surface can be stationary.

These are major limitations when dealing with complicated flows such as flow over a blade with film cooling holes and plenums. The plenum inlets are rarely axial. As a result of generating grids from GridPro, TURBO would have to deal with grids of arbitrary orientation in both the physical and computational coordinates.

Film Cooling

Several computations and experiments have been performed related to film cooling. This paper focuses on simulations of flow over a flat plate with one cooling hole at an angle of 35° fed by a plenum. The geometry is shown in Figure 1. Lemmon et al. (Ref. 3) studied the formation of counter rotating vortices for the case of a 35° hole. They found that the vortices are the result of the interaction between the jet and the mainstream and not the boundary layer vorticity of the cooling hole. The counter rotating or kidney shaped vortices are responsible for mixing the hot mainstream flow with the coolant. El-Gabry et al. (Ref. 4) performed this simulation using the NASA code Glenn-HT with the aim of identifying why CFD underestimates film cooling effectiveness. They found that CFD underpredicts the vertical mixing in the jet wake. Sinha et al. (Ref. 5) performed an experiment to quantify the film cooling effectiveness for the geometry shown in Figure 1. They performed the experiment for blowing ratios ranging from 0.25 to 1.0 and density ratios of 1.2, 1.6, and 2.0. They found that centerline effectiveness scales with momentum ratio while laterally averaged effectiveness is dependent on density ratio and momentum ratio. The results of the film cooling simulation in this report are compared to the work of Sinha et al. (Ref. 5) for the highest density ratio case (DR = 2.0). This paper does not present a detailed literature review because it primarily deals with code validation. A more detailed literature survey can be found in the work of El-Gabry et al.

Nomenclature

d	diameter of film cooling hole
DR	density ratio $= \rho_j / \rho_\infty$
k	turbulent kinetic energy
u	axial velocity
L	length of film cooling hole
M	blowing ratio $= \rho_j U_j / \rho_\infty U_\infty$
T	temperature
T_w	isothermal wall temperature
T_∞	mainstream inlet temperature
T_c	coolant temperature
T_{aw}	adiabatic wall temperature
VR	jet to mainstream velocity ratio $= U_j / U_\infty$
η	film effectiveness $= (T_\infty - T_{aw}) / (T_\infty - T_c)$
μ	viscosity
μ_T	turbulent viscosity
θ	dimensionless air temperature $= (T - T_\infty) / (T_c - T_\infty)$
ρ	density
ω	turbulent rate of dissipation

Modifications to TURBO

Wilcox's *k*-ω Turbulence model

Wilcox's *k*-ω turbulence model (Ref. 6) was incorporated into TURBO by adding the appropriate source terms into the general 2–equation turbulence model equation that is already implemented in TURBO. The general two-equation model is given by (Ref. 6),

$$(\mathrm{psi})_{,t} + (\rho s_i u_j + q_{ij})_{,j} = H_i$$

$$q_{ij} = -(\mu + \mu_T / Pr_i) s_{i,j}, i = 1,2.$$

Here, $s_1 = k$, $s_2 = \omega$ and $\mu_T = \alpha^* \rho k / \omega$. The source terms H are given by,

$$H_k = \mu_T \Omega^2 - \frac{2}{3}\tau\rho k - \beta^* \rho k \omega$$
$$H_\omega = \alpha\left(\mu_T \Omega^2 / k - \frac{2}{3}\tau\rho\right)\omega - \beta\rho\omega^2$$

where Ω is the vorticity. The coefficients in the model are as follows,

$$\mathrm{Pr}_k = \mathrm{Pr}_\omega = 2.0, \quad \beta = 3/40, \quad \beta^* = 0.09 F_\beta, \quad \alpha = (5/9)(F_\alpha / F_\mu)$$
$$F_\beta = \frac{5/18 + (\mathrm{Re}_T / R_\beta)^4}{1 + (\mathrm{Re}_T / R_\beta)^4}, \quad F_\alpha = \frac{\alpha_0 + \mathrm{Re}_T / R_\omega}{1 + \mathrm{Re}_T / R_\omega}, \quad F_\mu = \alpha_0 = \frac{\alpha_0^* + \mathrm{Re}_T / R_k}{1 + \mathrm{Re}_T / R_k}$$
$$\mathrm{Re}_T = \frac{\rho k}{\mu\omega}, \quad \alpha_0 = 0.1, \quad \alpha_0^* = 0.025, \quad R_\beta = 8, \quad R_\omega = 2.7, \quad R_k = 6.$$

The boundary conditions for a no slip surface are (Ref. 6), $k = 0$, $\omega = 100 \left.\frac{\partial u}{\partial y}\right|_{\mathrm{wall}}$. An upper limit (Ref. 6) of $(\omega_{\max})_{\mathrm{wall}} = \frac{800}{\mathrm{Re}} \frac{\nu}{(\Delta y)^2}$ was imposed at the wall to avoid large eddy viscosities in leading edge regions.

Boundary Conditions

Several modifications were made to TURBO to allow it to handle not only inlets and exits in different physical orientations (*x*,*y*,*z*) but also arbitrary computational (*i*,*j*,*k*) directions. Code was developed to study inlet and exit blocks and to determine whether or not the blocks are part of a flow passage with an identifiable hub and shroud. In the event of a hub and shroud being identified, the hub to shroud direction is specified as the direction for setting up radial profiles. If no hub to shroud direction is located, the code assigns uniform conditions at the inlet or exit. A plenum inlet boundary condition was added using general characteristic boundary conditions (Ref. 7). Figure 2 shows the stencil used for the plenum boundary condition and the symbol, *ℓ*, refers to an arbitrary computational index (*i*,*j*,*k*). It is assumed that the flow will enter the plenum inlet normal to the plenum inlet surface. The unit normal to the surface is given by (Ref. 8)

$$\vec{n} = \frac{1}{\sqrt{\xi_x^2 + \xi_y^2 + \xi_z^2}} \left(\xi_x \hat{i} + \xi_y \hat{j} + \xi_z \hat{k} \right)$$

Therefore the velocity component normal to the surface, just inside the computational domain is given by $u_{\text{in}} = \vec{V} \cdot \vec{n}$, where $\vec{V} = v_x \hat{i} + v_y \hat{j} + v_z \hat{k}$ is the velocity at l_{in}. The non-dimensional speed of sound, c_{in}, is calculated as $\sqrt{\left. \frac{\gamma p}{\rho} \right|_{\text{in}}}$. The Riemann invariants at l_{in} and l_b are related as

$$R_{\text{in}} = u_{\text{in}} - \frac{2c_{in}}{\gamma - 1} = R_b = u_b - \frac{2c_b}{\gamma - 1}$$

$$\therefore u_b = R_b + \frac{2c_b}{\gamma - 1} \tag{1}$$

The speed of sound at l_b is calculated as follows:

$$\frac{T_0}{T_b} = 1 + \frac{\gamma - 1}{2} M_b^2$$

$$T_b = c_b^2; \quad M_b = \frac{u_b}{c_b}$$

$$\therefore c_b^2 = T_0 - \frac{\gamma - 1}{2} u_b^2 \tag{2}$$

Now, substituting Equation (1) in Equation (2) leads to

$$c_b^2 = T_0 - \frac{\gamma - 1}{2} \left(R_b + \frac{2c_b}{\gamma - 1} \right)^2 \tag{3}$$

This is a quadratic equation in c_b that is easily solved (Ref. 8) and substituting back into Equation (1) gives u_b. The individual velocity components, density and pressure at the phantom cell are then computed as

$$\vec{V}_b = \frac{u_b}{\sqrt{\xi_x^2 + \xi_y^2 + \xi_z^2}} \left(\xi_x \hat{i} + \xi_y \hat{j} + \xi_z \hat{k} \right) \tag{4}$$

$$\rho_b = \frac{\gamma P_0}{T_0}$$

$$P_b = \frac{P_0}{\left(1 + \frac{\gamma - 1}{2} M_b^2 \right)^{1/\gamma - 1}}$$

It is also possible to specify multiple inlet pressures and temperatures through the input files (for cases having more than one inlet and/or exit). This will allow users to specify a plenum temperature and pressure that are different from the inlet pressure and temperature of the blade row. For film cooling applications where the plenum pressure is close to the main flow pressure and the density ratio is high, it is possible for backflow to occur during convergence. This can lead to failure of the simulation. To avoid this scenario, the speed of sound, c_b, in Equation (3) was modified to $c_b = |c_b|$ and u_b in Equation (4) was replaced with $|u_b|$ to force flow to enter the plenum normal to the plenum inlet face and therefore aid in convergence. Inlet and exit mass flux calculations were updated to accurately display mass flux regardless of the inlet and exit direction. Slip and no slip boundary conditions were also updated to enable them to handle directional generality. In addition, minor modifications in the treatment of viscous fluxes and in the calculation of pressure and energy in phantom cells were implemented. To enable the study of heat transfer, an isothermal boundary condition has been implemented. The temperature at the phantom cell is calculated by assuming that the wall temperature is the average of the phantom cell temperature and the inside cell temperature.

$$P_{\text{in}} = e - \frac{\gamma - 1}{2}\left(\left|\vec{V}\right|^2\right)$$

$$T_{\text{in}} = \frac{\gamma P_{\text{in}}}{\rho_{\text{in}}}$$

$$T_{\text{phantom}} = 2T_{\text{in}} - T_{\text{wall}}$$

$$\rho_{\text{phantom}} = \frac{\gamma P_{\text{phantom}}}{T_{\text{phantom}}}$$

The wall temperature is specified as user input.

Simulations and Results

Flat Plate

A 2–D channel grid (Ref. 8), shown in Figure 3, was used to model flow over a flat plate by imposing a no slip boundary condition on only one of the two channel walls while maintaining a slip boundary on the other wall. TURBO, designed to handle internal flows, is currently unable to accommodate multiple exit boundaries in one block of the grid. The grid was divided into four blocks, as shown in Figure 3, with each block containing 41 points in the *i*-direction (local *x* coordinate), 31 points in the *k*-direction (local negative *y* coordinate) and 2 points in the *j*-direction (local negative *z* coordinate).
Here, the positive *x* direction is taken to be the downstream direction.

The leading edge of the flat plate is located at $i = 31$, $k = 31$, $j = 1$ to 2 in block 2 and the trailing edge is at $i = 41$, $k = 31$, $j = 1$ to 2 in block 4. The flat plate is 1.46 m long and the channel height is approximately 0.021 m. The grid spacing ensures a y+ of approximately 1 at the first grid point away from the surface of the flat plate.

A no-slip boundary condition was imposed on the flat plate. Radial equilibrium was imposed on the exit plane while a characteristic variable inlet boundary was established on the inlet plane. The flow was initialized uniformly with a Mach number of 0.3 and a back pressure of 98000 Pa with total pressure taken to be atmospheric. For the turbulence model, k and ω were specified at the inlet based on the inlet

turbulence intensity, Tu, the inlet velocity, u_i and the turbulent length scale, l. The turbulent intensity at the inlet was specified to be 5 percent. However, the turbulence intensity was initialized to 1 percent to ensure stable running of the code. The code was run at a Courant-Friedrichs-Levy (CFL) number of five.

The solutions obtained by running TURBO were deemed to be fully converged when successive iterations varied by less than 0.1 percent in velocity gradient and temperature gradient. For the case of an adiabatic flat plate, skin friction coefficients were computed based on wall shear stress and free stream dynamic pressure. For the case of an isothermal flat plate local Nusselt numbers were computed based on the temperature difference between the local wall temperature and total temperature and the conductivity at the wall. For laminar flow, velocity profiles were compared to those of Blasius' (Ref. 9) solution for both an isothermal and an adiabatic flat plate.

Figure 4 shows that TURBO predicts fairly well, for Reynolds numbers between 10^5 and 10^7, the skin friction coefficient in both turbulent and laminar flow over a flat plate with no heat transfer at the surface. Small deviations can be attributed to compressibility effects that are neglected in the theoretical solution of Blasius. These compressibility effects become more obvious when the plate is held at a constant wall temperature, T_w, of 0.7 relative to the free stream (see Fig. 5). This is due to the strong dependence of kinematic viscosity on temperature.

Further evidence of this can be seen in Figure 6, where the wall temperature is held at 0.9 relative to the free stream. Agreement with theory is clearly much improved for both laminar and turbulent flow.

Nusselt numbers for the case of $T_w = 0.9$ matched well with theory, for $5 \cdot 10^5 < \mathrm{Re} < 10^7$, showing the excellent heat transfer prediction of the k-ω turbulence model at least for the simple case of a flat plate. At a wall temperature of $T_w = 0.7$, compressibility effects cause deviation of TURBO results from theory. Figures 7 and 8 show local Nusselt numbers for $T_w = 0.7$ and $T_w = 0.9$, respectively. Figures 9 and 10 show a velocity profile comparison with theory for laminar flow over an isothermal flat plate and over an adiabatic flat plate, respectively. Here, $\eta = 0.5y\left(U_e / \nu x\right)^{0.5}$, is the Blasius similarity variable (Ref. 9). The anomalous spike circled in Figure 5 and seen in the remaining figures occurs at a block interface and is a result of calculating derivatives (such as temperature gradient and velocity gradient) using the post processor FIELDVIEW (Intelligent Light).

Film Cooling

In order to test the modifications made to TURBO, a simulation was run using a fine grid representing a flat plate with a cooling hole and plenum. Figure 12 shows the computational grid and boundary conditions. The boundaries not explicitly labeled in Figure 12 were assigned slip boundary conditions. The cooling hole is inclined at 35° to the freestream as shown in Figure 13. The domain was partitioned into 19 blocks and each block was run on a single processor. The flow was initialized as laminar with a Mach number of 0.0 and back pressure of approximately 97 percent of the inlet stagnation pressure. A converged solution obtained from this laminar flow simulation was then utilized as initialization for a turbulent flow simulation. Table 1 shows the cases for which results are shown in this paper and the plenum inlet conditions corresponding to them.

The turbulent flow simulation employed Wilcox's k-ω turbulence model previously described in this report. The results obtained showed qualitative agreement with experiments and quantitative agreement with the film cooling work of other researchers such as El-Gabry et al., Figure 14 shows span averaged film cooling effectiveness for cases 1-3. The data represented in these figures is that of Sinha et al. (Ref. 5). Here, $x = 0.0$ corresponds to the leading edge of the hole and $x = 1.0$ is the trailing edge of the hole. For the lower density ratio, agreement with experiment is quite good downstream of the hole but not near the hole exit. The cooling effectiveness is under-predicted downstream of the hole but agreement with data is better closer to the hole exit. This is thought to be a result of the linear turbulence model currently being utilized that is unable to account for the swirl at the hole exit. Similar behavior is observed in the literature, for example, El-Gabry et al. (Ref. 4). Figure 15 shows contours of non-dimensional temperature for case 3 along the centerline. this agrees well with the results of El-Gabry et al.

Figure 16 shows a cross section of the flow at $x/d = 3.0$ for case 3 to show the kidney shaped vortex. Figure 17 shows streamlines in the vicinity of the hole exit. While mixing occurs in the near hole region, the streamlines from the hole can be seen to lift off downstream of the hole thereby reducing effectiveness.

Conclusions

Modifications to TURBO have been successfully validated by running simulations for flow over an isothermal and an adiabatic flat plate as well as flow over a flat plate cooled by a 35° film cooling hole. For the flat plate, heat transfer results matched well with theory. For the film cooling simulation, good qualitative agreement with experiment was observed. The quantitative differences between film effectiveness computed from the simulation and that from experiment are consistent with current literature and are thought to be a result of the turbulence model. The heat transfer capability of TURBO as well as its ability to simulate film cooling have been demonstrated to be at par with modern simulation capabilities.

References

1. Chen, J.P., and Briley, W.R., "A Parallel Flow Solver for Unsteady Multiple Blade Row Turbomachinery Simulations," ASME–2001–GT–0348. June 2001.
2. Herrick, G.P., "Facilitating Higher Fidelity Simulations of Axial Compressor Instability and Other Turbomachinery Flow Conditions," PhD Thesis, May 2008, Mississippi State University.
3. Lemmon, C.A., Kohli, A. and Thole, K.A., "Formation of Counter-Rotating Vortices in Film Cooling Flows," Pratt & Whitney, 400 Main Street, MS 169-02, East Hartford, CT 06108.
4. El-Gabry, L., Heidmann, J. and Ameri, A., "Numerical Analysis of Film Cooling at High Blowing Ratio," April 2009, NASA/TM—2009-215517.
5. Sinha, A.K., Bogard, D.G., and Crawford, M.E., 1991, "Film-Cooling Effectiveness Downstream of a Single Row of Holes with Variable Density Ratio," Journal of Turbomachinery, Vol. 113, pp. 442–449.
6. Garg, V.K., Ameri, A., "Comparison of two-equation turbulence models for prediction of heat transfer on film cooled turbine blades," AYT Corporation, Cleveland OH, 1997.
7. Whitfield, D.L, Janus, J.M., 1984, Three-Dimensional Unsteady Euler Equations Solution Using Flux Vector Splitting, Department of Aerospace Engineering, Mississippi State University.
8. Chen, J.P., "Unsteady three-dimensional thin-layer NAVIER-Stokes solutions for turbomachinery in transonic flow," PhD thesis, Mississippi State University, Mississippi, 1991.
9. Young, A.D., "Bundary Layers," AIAA Education Series, 1989.

TABLE 1.—TEST CASES AND PLENUM INLET CONDITIONS

Case	Plenum inlet Stagnation pressure	Plenum inlet Stagnation temperature	Density ratio	Blowing ratio
1	0.966	0.516	2.0	0.5
2	0.986	0.516	2.0	0.8
3	1.009	0.52	2.0	1.0

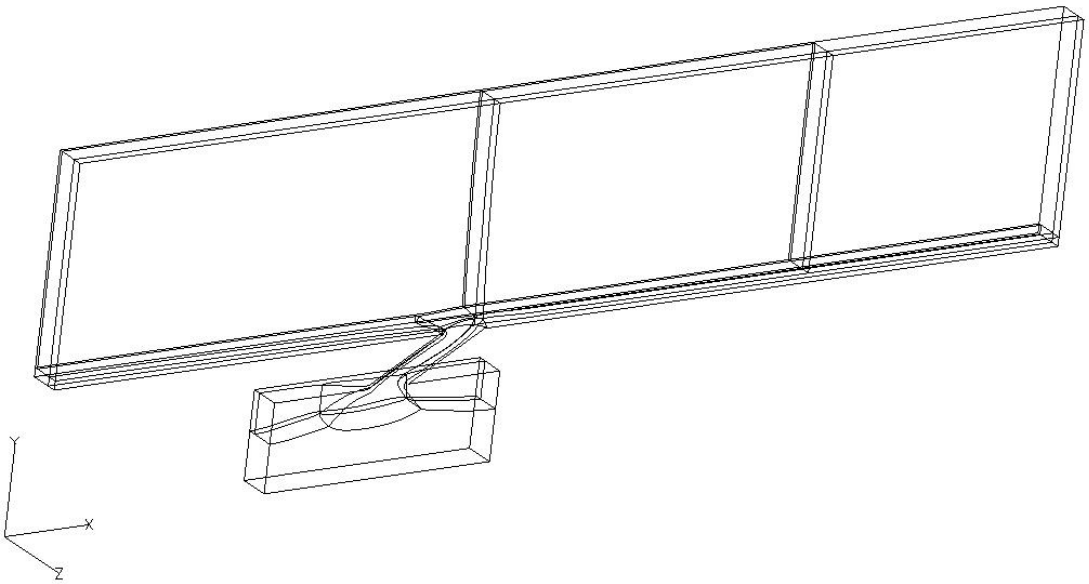

Figure 1.—Computational domain.

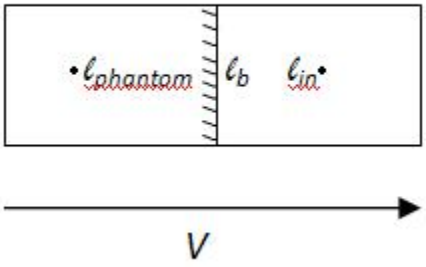

Figure 2.—Boundary condition stencil.

Figure 3.—Mesh for 2–D flow over flat plate.

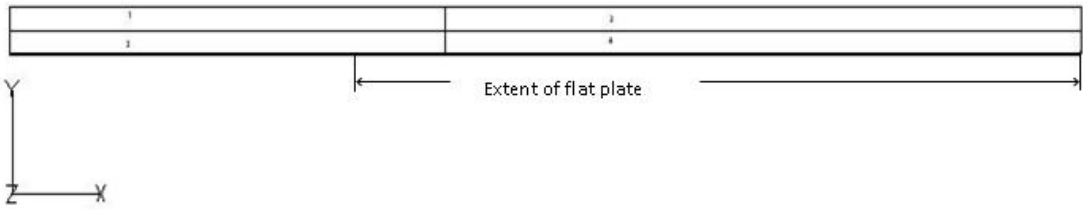

Figure 4.—Block structure and extent of flat plate.

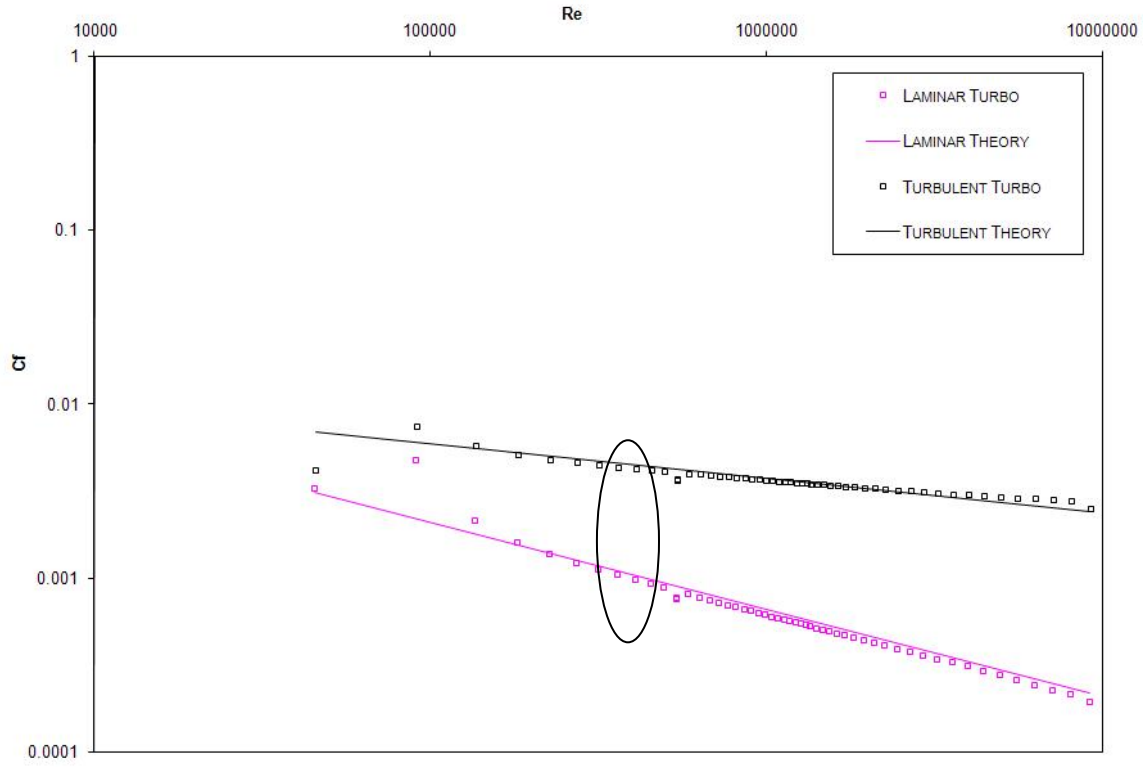

Figure 5.—Logarithmic plot of local skin friction coefficient versus Reynolds number for an adiabatic flat plate.

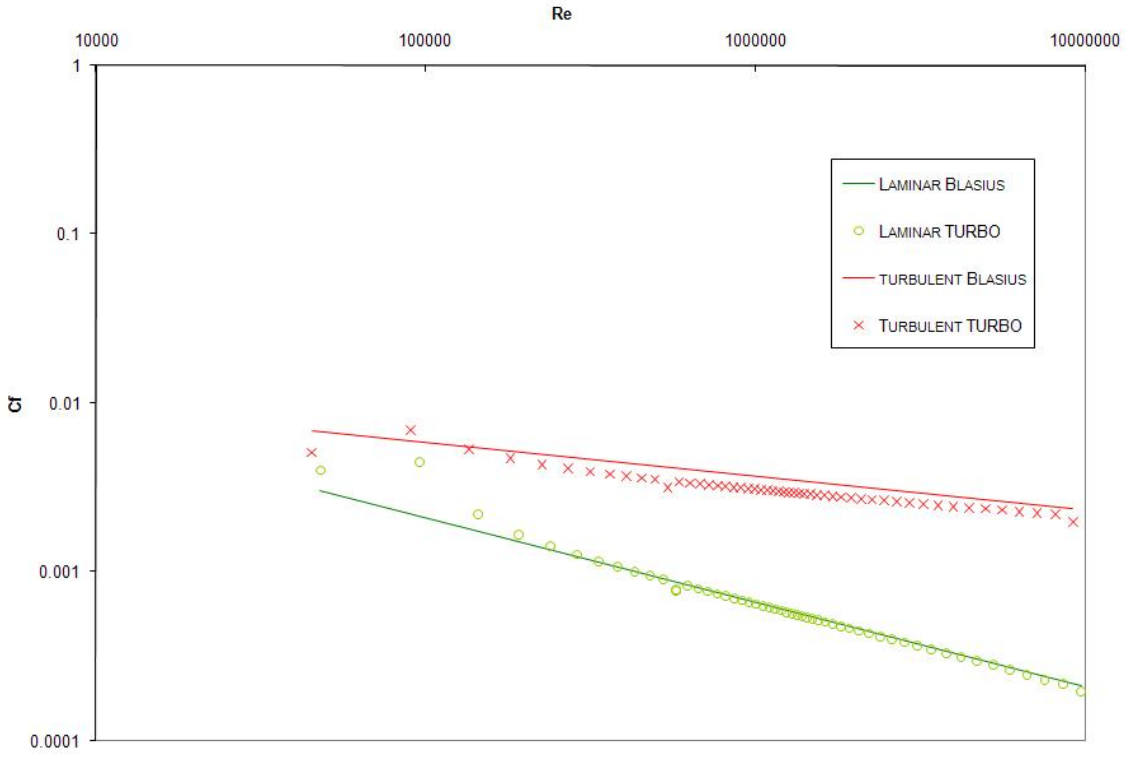

Figure 6.—Logarithmic plot of local skin friction coefficient versus Reynolds number for *Tw* = 0.7.

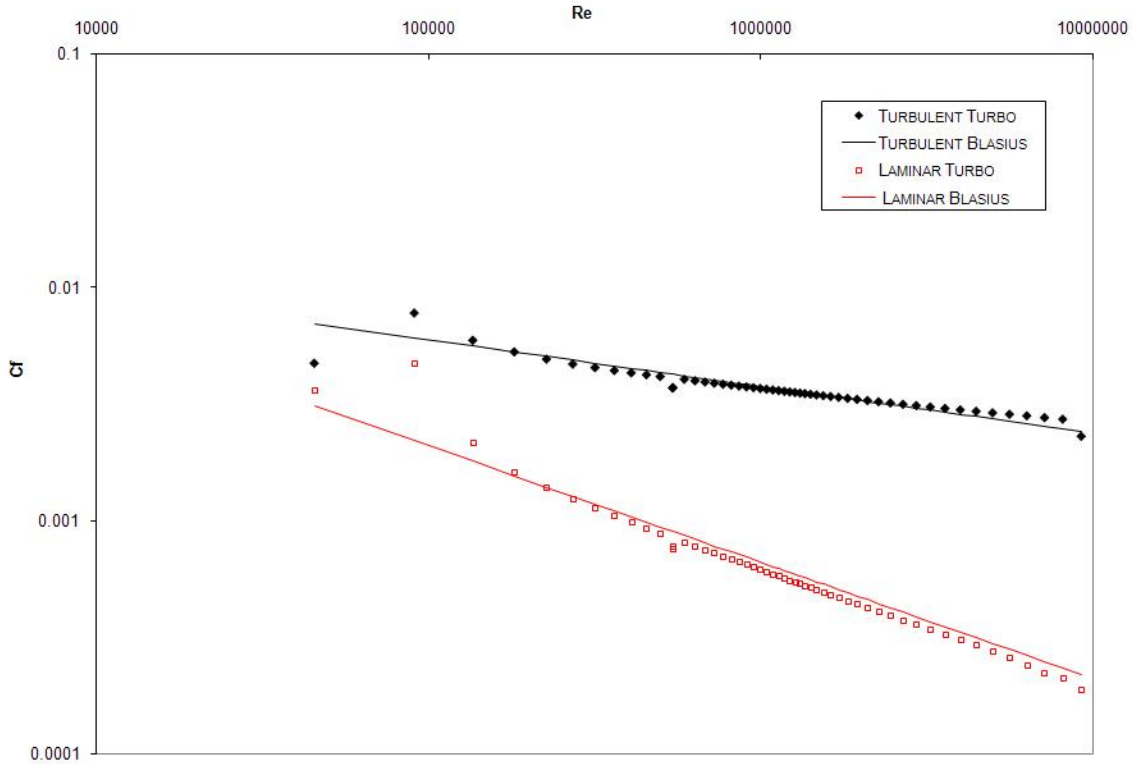

Figure 7.—Logarithmic plot of local skin friction coefficient versus Reynolds number for *Tw* = 0.9.

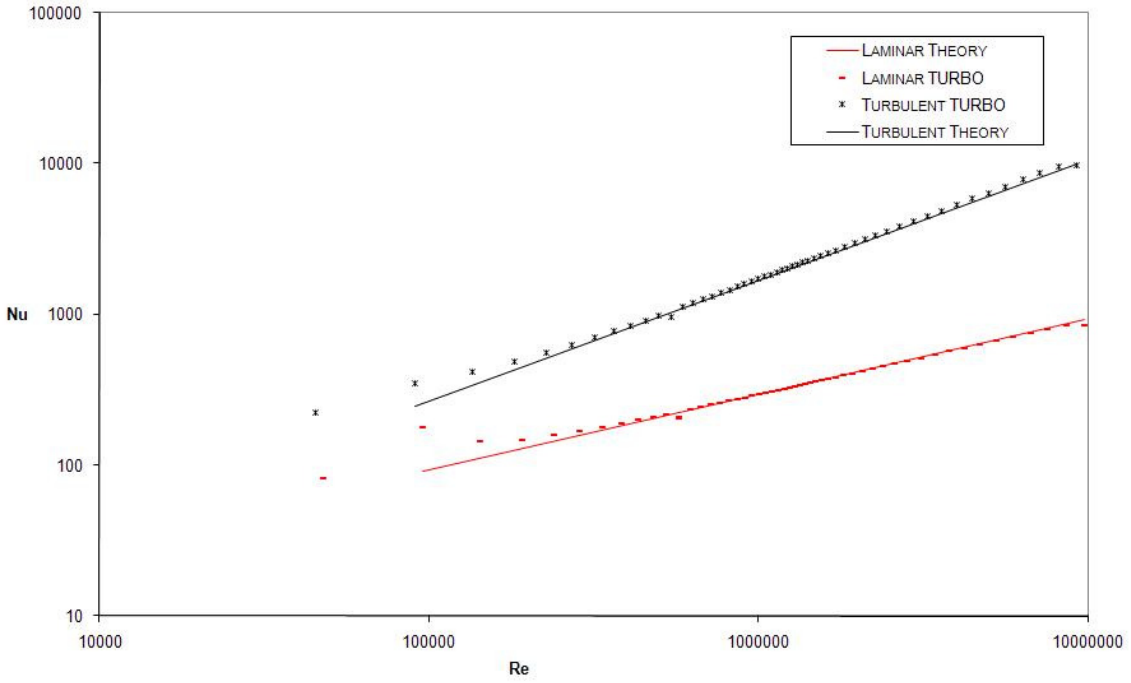

Figure 8.—Logarithmic plot of local Nusselt number versus Reynolds number for *Tw* = 0.7.

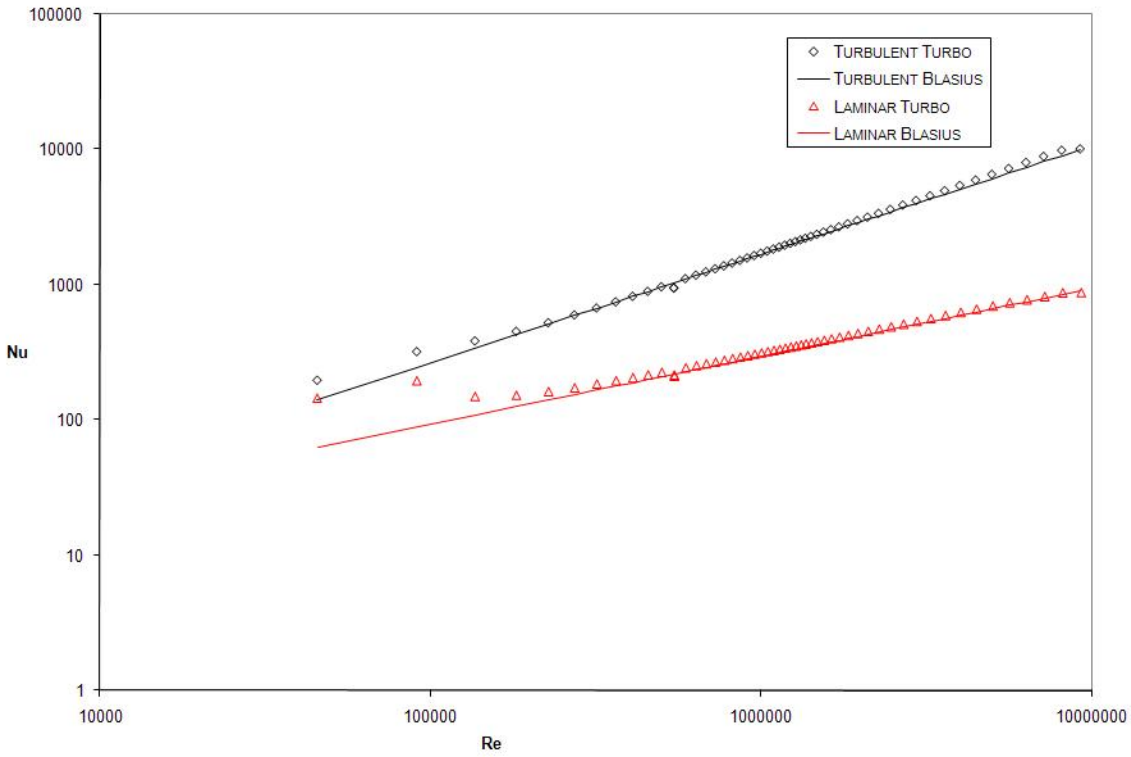

Figure 9.—Logarithmic plot of local Nusselt number versus Reynolds number for *Tw* = 0.9.

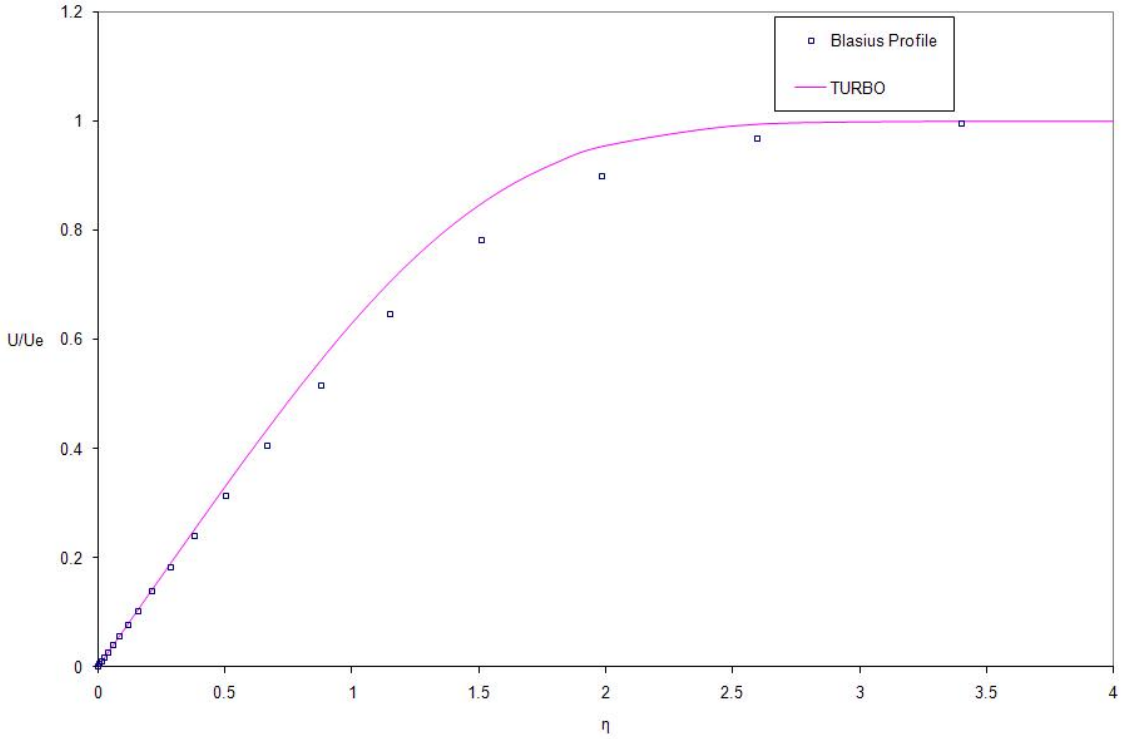

Figure 10.—Velocity profile for laminar flow over an isothermal flat plate with *Tw* = 0.7.

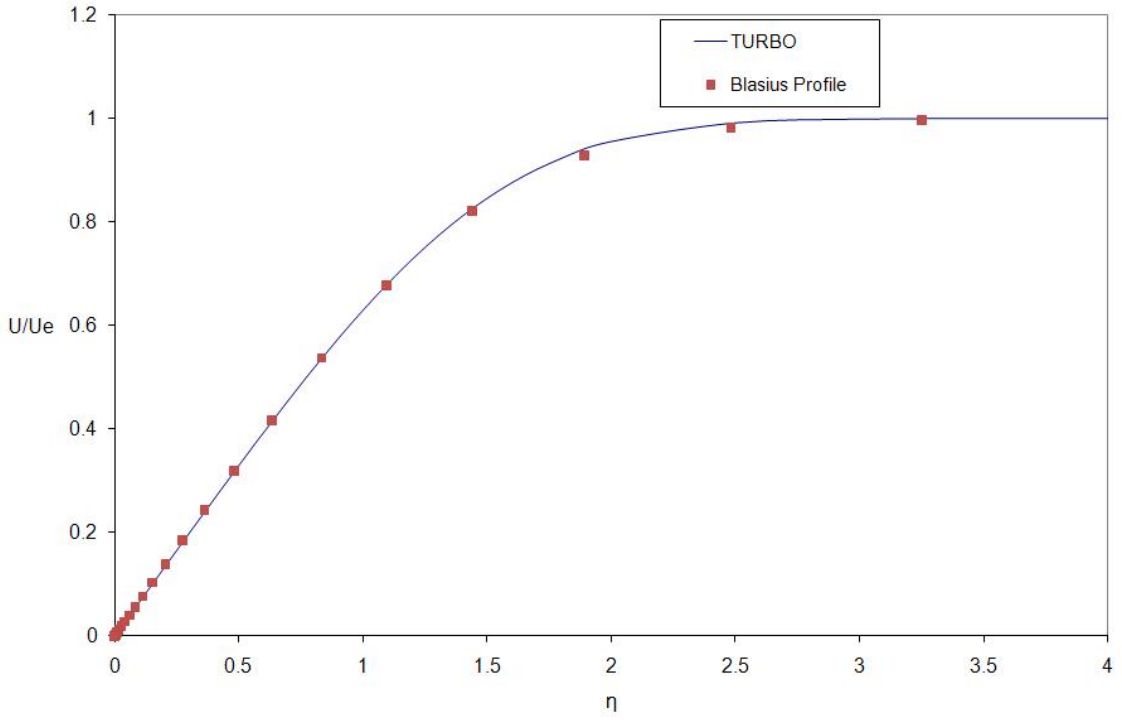

Figure 11.—Velocity profile for laminar flow over an adiabatic flat plate.

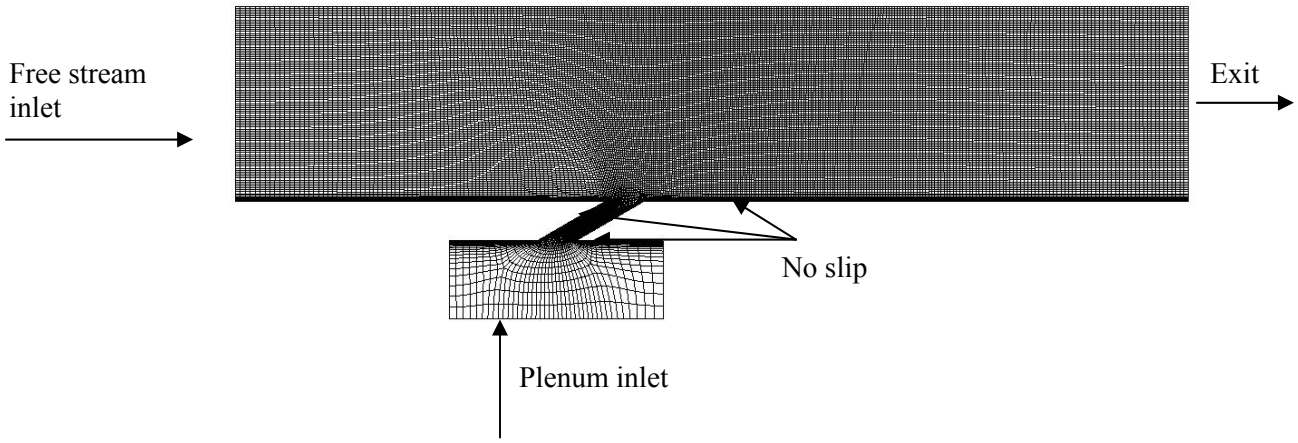

Figure 12.—Mesh for 35° cooling hole.

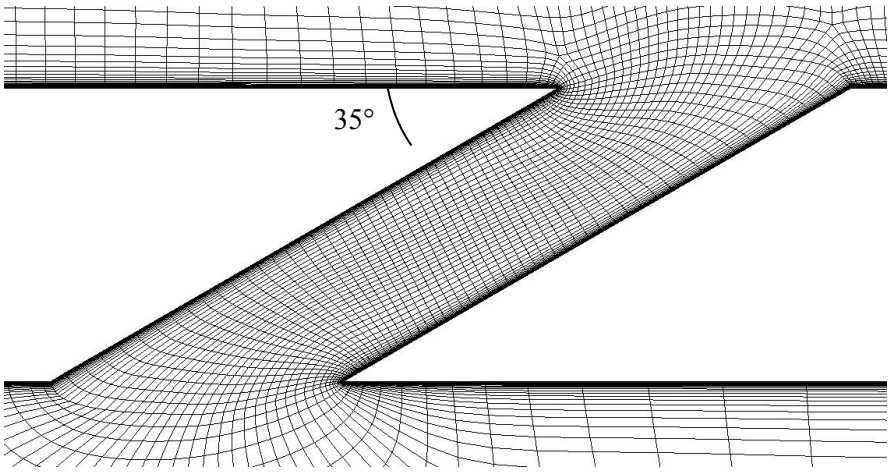

Figure 13.—Grid in cooling hole region.

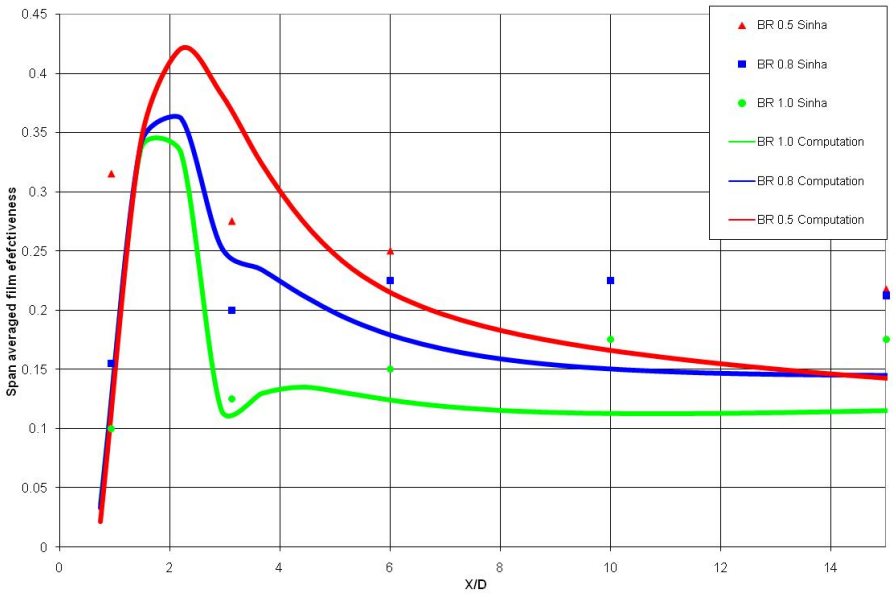

Figure 14.—Span averaged film effectiveness at density ratio of 2.0.

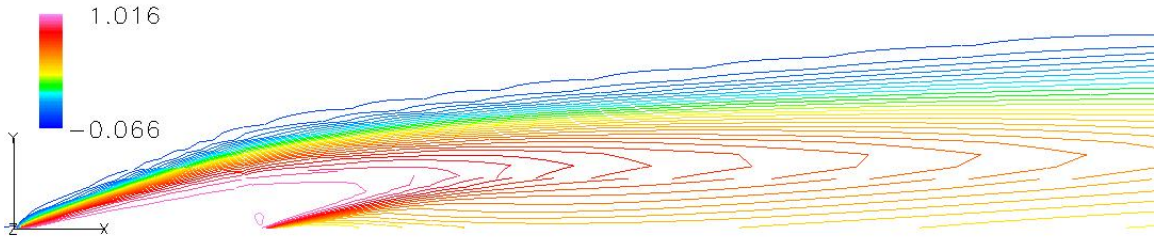

Figure 15.—Contours of non-dimensional temperature at centerline for case 3.

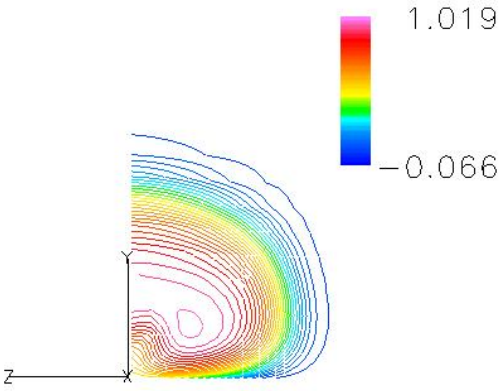

Figure 16.—Kidney shaped vortex at x/d = 3.0 for case 3.

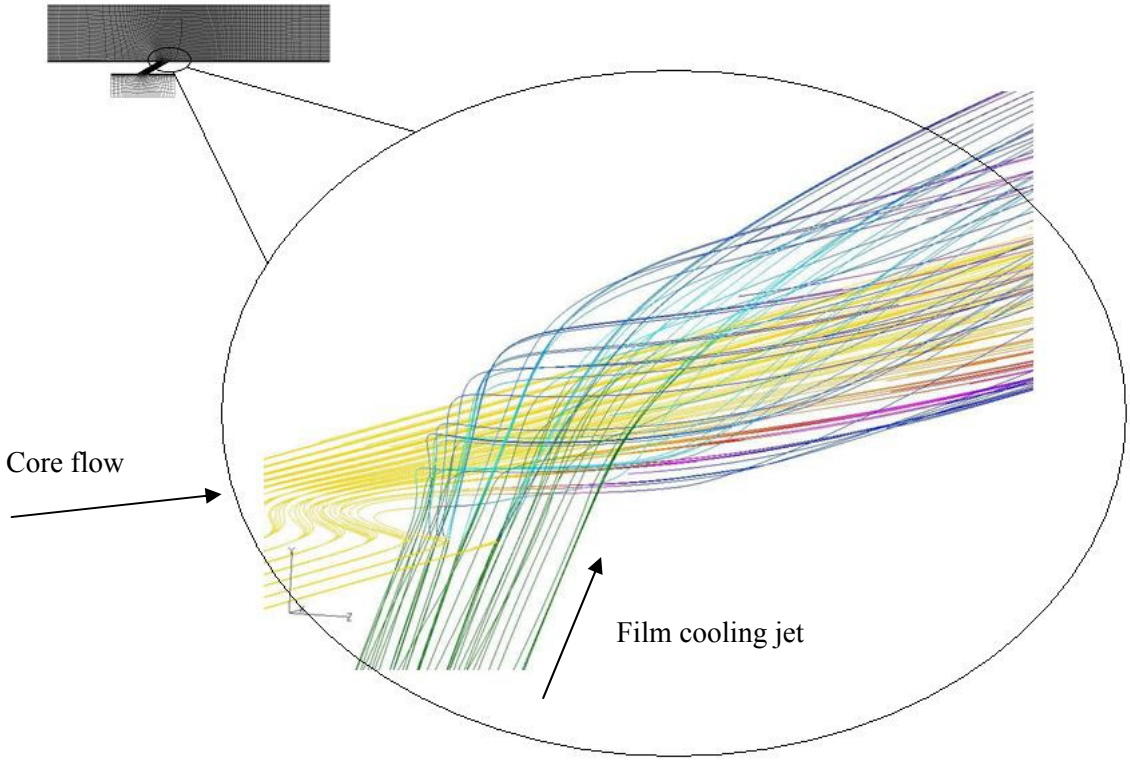

Figure 17.—Streamlines in the vicinity of the hole exit.

REPORT DOCUMENTATION PAGE		Form Approved OMB No. 0704-0188

1. REPORT DATE *(DD-MM-YYYY)*	2. REPORT TYPE	3. DATES COVERED *(From - To)*
01-06-2010	Technical Memorandum	

4. TITLE AND SUBTITLE
Validation of Heat Transfer and Film Cooling Capabilities of the 3-D RANS Code TURBO

5a. CONTRACT NUMBER

5b. GRANT NUMBER

5c. PROGRAM ELEMENT NUMBER

6. AUTHOR(S)
Shyam, Vikram; Ameri, Ali; Chen, Jen-Ping

5d. PROJECT NUMBER

5e. TASK NUMBER

5f. WORK UNIT NUMBER
WBS 561581.02.08.03.21.03

7. PERFORMING ORGANIZATION NAME(S) AND ADDRESS(ES)
National Aeronautics and Space Administration
John H. Glenn Research Center at Lewis Field
Cleveland, Ohio 44135-3191

8. PERFORMING ORGANIZATION REPORT NUMBER
E-17315

9. SPONSORING/MONITORING AGENCY NAME(S) AND ADDRESS(ES)
National Aeronautics and Space Administration
Washington, DC 20546-0001

10. SPONSORING/MONITOR'S ACRONYM(S)
NASA

11. SPONSORING/MONITORING REPORT NUMBER
NASA/TM-2010-216738

12. DISTRIBUTION/AVAILABILITY STATEMENT
Unclassified-Unlimited
Subject Categories: 02, 34, and 61
Available electronically at http://gltrs.grc.nasa.gov
This publication is available from the NASA Center for AeroSpace Information, 443-757-5802

13. SUPPLEMENTARY NOTES

14. ABSTRACT
The capabilities of the 3-D unsteady RANS code TURBO have been extended to include heat transfer and film cooling applications. The results of simulations performed with the modified code are compared to experiment and to theory, where applicable. Wilcox's *k*-ω turbulence model has been implemented to close the RANS equations. Two simulations are conducted: (1) flow over a flat plate and (2) flow over an adiabatic flat plate cooled by one hole inclined at 35° to the free stream. For (1) agreement with theory is found to be excellent for heat transfer, represented by local Nusselt number, and quite good for momentum, as represented by the local skin friction coefficient. This report compares the local skin friction coefficients and Nusselt numbers on a flat plate obtained using Wilcox's *k*-ω model with the theory of Blasius. The study looks at laminar and turbulent flows over an adiabatic flat plate and over an isothermal flat plate for two different wall temperatures. It is shown that TURBO is able to accurately predict heat transfer on a flat plate. For (2) TURBO shows good qualitative agreement with film cooling experiments performed on a flat plate with one cooling hole. Quantitatively, film effectiveness is under predicted downstream of the hole.

15. SUBJECT TERMS
Heat transfer; Film cooling; Turbulence model

16. SECURITY CLASSIFICATION OF:			17. LIMITATION OF ABSTRACT	18. NUMBER OF PAGES	19a. NAME OF RESPONSIBLE PERSON
a. REPORT	b. ABSTRACT	c. THIS PAGE			STI Help Desk (email:help@sti.nasa.gov)
U	U	U	UU	21	19b. TELEPHONE NUMBER *(include area code)* 443-757-5802